RNA condensates as platforms for prebiotic chemistry

Samuel Hauf,[†] Ryo Nakamura,[‡] Barbara Cellini,[¶] Yohei Yokobayashi,[†] and Mirco Dindo[*,¶]

†*Okinawa Institute of Science and Technology Graduate University, Okinawa, Japan*

‡*Ushimado Marine Institute, Faculty of Science, Okayama University, Okayama, Japan*

¶*Università degli Studi di Perugia, Department of Medicine and Surgery, Perugia, Italy*

E-mail: mirco.dindo@unipg.it

Phone: +39-0755858195

Abstract

The emergence of the first catalytically active biopolymers remains a scientific mystery. Some abiotic chemistries for the formation of precursor molecules to biopolymers — such as nucleotides and amino acids — are known. However, abiotic polymerization usually results in short polymers of only a few units in length. This is too short for meaningful information storage or catalytic activity, a limitation known as the Flory Length Problem. Additionally, the first biocatalysts presumably had low activity because they were generated by random polymerization. Therefore, enrichment of substrates and catalysts seems necessary for significant rates of catalysis to occur. Could RNA phase separation be a solution to these challenges? Our experimental evidence demonstrates that at acidic pH, short RNAs (<20 nt) readily phase-separate into a condensed phase enriched with longer RNA fragments, primarily through phosphate backbone protonation. These RNA condensates stably compartmentalize RNA and

DNA species without rapid flux of genetic material, maintaining their identity over extended periods even in the absence of membranes. In addition, the RNA phase concentrates ions critical for RNA folding and activity, along with small organic molecules, phospholipids, peptides, ribozymes, and large proteins. Beyond enriching diverse components, RNA condensates function as microreactors with dual catalytic capabilities. They physically enhance reaction rates by concentrating reactants within a confined space and simultaneously act as inherent catalysts that directly facilitate chemical transformations. These condensates also support ribozyme and enzymatic activity. Collectively, these findings suggest that RNA phase separation may have played a crucial role in life's origins by providing spatial compartmentalization, inherent catalytic activity, and biopolymer enrichment, particularly of potentially longer catalytic species.

Introduction

Many biomolecules — like nucleic acids, proteins, lipids, and cofactors — are necessary to sustain the complex biochemistry that powers living organisms. However, how these lifeless components initially assembled to form the first active entities remains one of science's unanswered questions. The RNA world hypothesis[1] offers a potential explanation by proposing that life began with assemblies composed entirely of RNA that functioned as both information carrier and catalyst.[2,3] This hypothesis has gained significant traction in origin of life research due to the remarkable chemical versatility of RNA.[2,4–6]

Despite its explanatory power, the RNA world hypothesis faces several significant challenges.[7–9] It does not explain how information-encoding or catalytically active RNAs originally emerged. Known prebiotic chemistry cannot efficiently catalyze the formation of long RNA polymers from monomers. Instead, prebiotic reactions typically yield short oligomers a few nucleotides in length,[10] with polymer extension becoming increasingly improbable with each additional nucleotide — the "Flory Length Problem".[11] Furthermore, RNA is often considered too complex and unstable for prebiotic environments,[7,12] although recent evidence

suggests that RNA might have been stable under acidic conditions of the early Hadean eon.[13]

Another critical challenge is the catalytic efficiency of early biopolymers. Randomly polymerized RNA or protein catalysts would have initially existed at extremely low concentrations with minimal catalytic activity. Such unspecialized catalysts require high substrate and catalyst concentrations to function effectively.[7,9,12]

Compartmentalization provides a potential solution by concentrating key molecules and creating discrete units for natural selection.[14–17] To explain how chemicals could be organized into life-like assemblies, various protocell models have been proposed.[18–23] Compartments with membranes based on lipids or peptides are commonly considered plausible protocells,[24,25] but they present significant limitations. Membrane impermeability to polar charged molecules creates barriers for protometabolism and information flow.[26,27] In addition, such protocells require the simultaneous presence of at least two chemically distinct species (RNA plus lipids or peptides), which decreases the probability of spontaneous assembly in prebiotic environments.

Membrane-less compartments formed through liquid-liquid phase separation (LLPS) offer a potential alternative.[28,29] In LLPS, a solution of previously miscible components spontaneously forms two distinct coexisting liquid phases: a dense phase enriched in specific components and a surrounding dilute phase depleted of these components. Progress has been made in producing membrane-less systems from various biomolecules,[30–37] with some demonstrating division,[33,38] migration,[39] and out-of-equilibrium behaviors.[40,41] Although various membrane-less systems have been proposed, they typically require multiple distinct biopolymers or specific environmental conditions that are unlikely to coexist in prebiotic settings. Recently, it has been suggested that the RNA condensates themselves could have been catalytically active, forming the units that drove early evolution at the origin of life.[42]

Our work experimentally explores how RNA alone can form membrane-less compartments through phase separation (Fig. 1a). Using commercially available yeast RNA preparations as a surrogate for short RNA sequences, we observed spontaneous RNA condensation under

acidic conditions through phosphate backbone protonation. As illustrated in Fig. 1b, these RNA condensates exhibit several properties crucial to the origin of life. First, they selectively concentrate longer RNA species, potentially offering a solution to the Flory Length Problem. Second, they stably compartmentalize RNA in the absence of a membrane, without observable exchange of compartmentalized nucleic acids between different condensate populations, even during long-term merging events. This stability preserves distinct genetic identities — an essential prerequisite for evolution. Third, a wide range of molecules partition into their interior. This partitioning allows substrates as well as catalysts to be enriched, addressing the efficiency problem of early catalysis.

We further demonstrate that the RNA condensates support non-enzymatic catalysis through distinct mechanisms. The enrichment of molecules within the condensates significantly enhances catalytic efficiency. Additionally, the RNA condensates act as inherent catalysts themselves, due to their intrinsic chemical properties. In addition to enhancing non-enzymatic biochemical reactions, the RNA condensates also support complex biocatalysis by ribozymes and multi-subunit enzymes, improving their potential as vessels for primitive metabolism. Intriguingly, RNA condensates spontaneously interact with short-chain fatty acids to form hydrophobic surface layers (representing a potential bridge to primordial membranes), while phospholipids introduced to these systems form circular sub-structures within the condensates, further increasing their molecular complexity.

As depicted in Fig. 1, RNA condensates could serve as nucleation points for increasing complexity, selectively enriching nucleotides, peptides, and lipids, allowing the emergence of more sophisticated functions. The encapsulation of diverse biomolecules within initially membrane-less protocells could have created the conditions necessary for primitive metabolism and replication, initiating cycles of mutation and selection that drove biological evolution. Our observations suggest a pathway linking prebiotic chemistry to the RNA world. This link of chemistry to biology by RNA phase separation could potentially solve the challenges of concentration, compartmentalization, and catalysis at the origin of life.

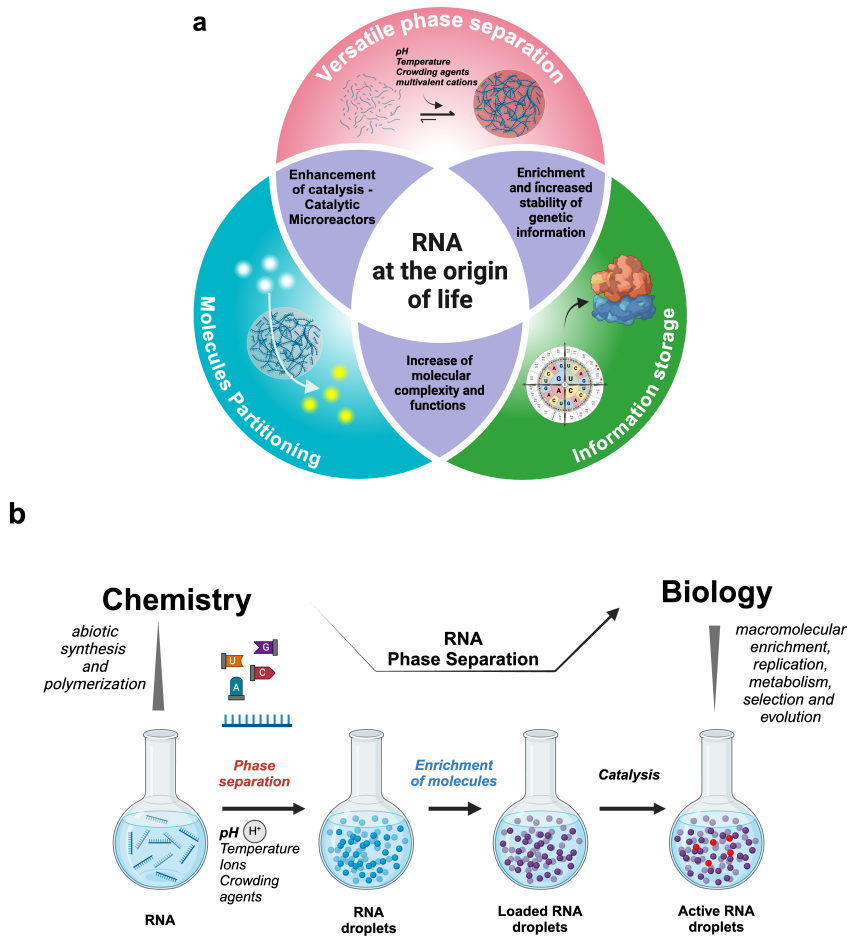

Figure 1: **Graph representing how RNA can contribute to the formation of primordial entities. a** Schematic representation of the main features of RNA at the origin of life. **b** Schema illustrating how RNA could generate phase-separated condensates which, by enriching other molecules, become catalytically active, and increase their complexity through the production of new molecules.

Results and discussion

RNA phase separation

RNA is an acid consisting of a hydrophilic sugar-phosphate backbone and hydrophobic nucleobases (Fig. 2 top). Concentrated nucleic acid solutions readily undergo phase separation upon dehydration.[43] We show that in addition to dehydration, RNA solutions close to saturation easily phase-separate under a variety of conditions. Details on the RNA used can be found in the supplementary information (Section **"Characterization and identity of phase-separated RNA"** and Fig. S1). Storing concentrated RNA solutions (5-10 g/L) on ice causes them to become turbid with numerous condensate droplets visible under the microscope (Fig. 2, middle). The addition of multivalent cations, such as magnesium (Fig. 2, right and Fig. 3a)[44–47] and others reported in Fig. S2, also triggers the phase separation of RNA in a concentration-dependent manner. We observed that a minimum of 25 mM $MgCl_2$ is required to induce phase separation at RNA concentrations as low as 0.5 g/L (Fig. 3a, heatmap).

Remarkably, RNA phase separation occurs even more readily when strong acids are added. Hydrochloric acid (pK_a gas -5.9) is particularly effective (Fig. 2, left), inducing phase separation at concentrations as low as 10 mM even with minimal RNA concentrations (around 0.237 g/L; Fig. 3a). The critical role of pH in RNA phase separation is evident when manipulating buffer composition (Fig. 3b,c). Increasing the pH by titrating with Tris-HCl buffer (pH 7.0 or 8.0) dramatically reduces both the size and number of RNA condensates (Fig. S3), leading to complete dissolution above pH 4.5-5.0 (Fig. 3c).

To further investigate the relationship between acidity and RNA phase separation, we tested acids with different pK_a values (Fig. 3d). Strong acids such as nitric acid (pK_a 1.4), or sulfuric acid (pK_{a1} = 2.8, pKa2 = 1.99) efficiently induce RNA phase separation, whereas weaker organic acids like formic acid (pK_a 3.745) and acetic acid (pK_a 4.756) do not trigger RNA phase separation. By correlating pH measurements with absorbance data, we

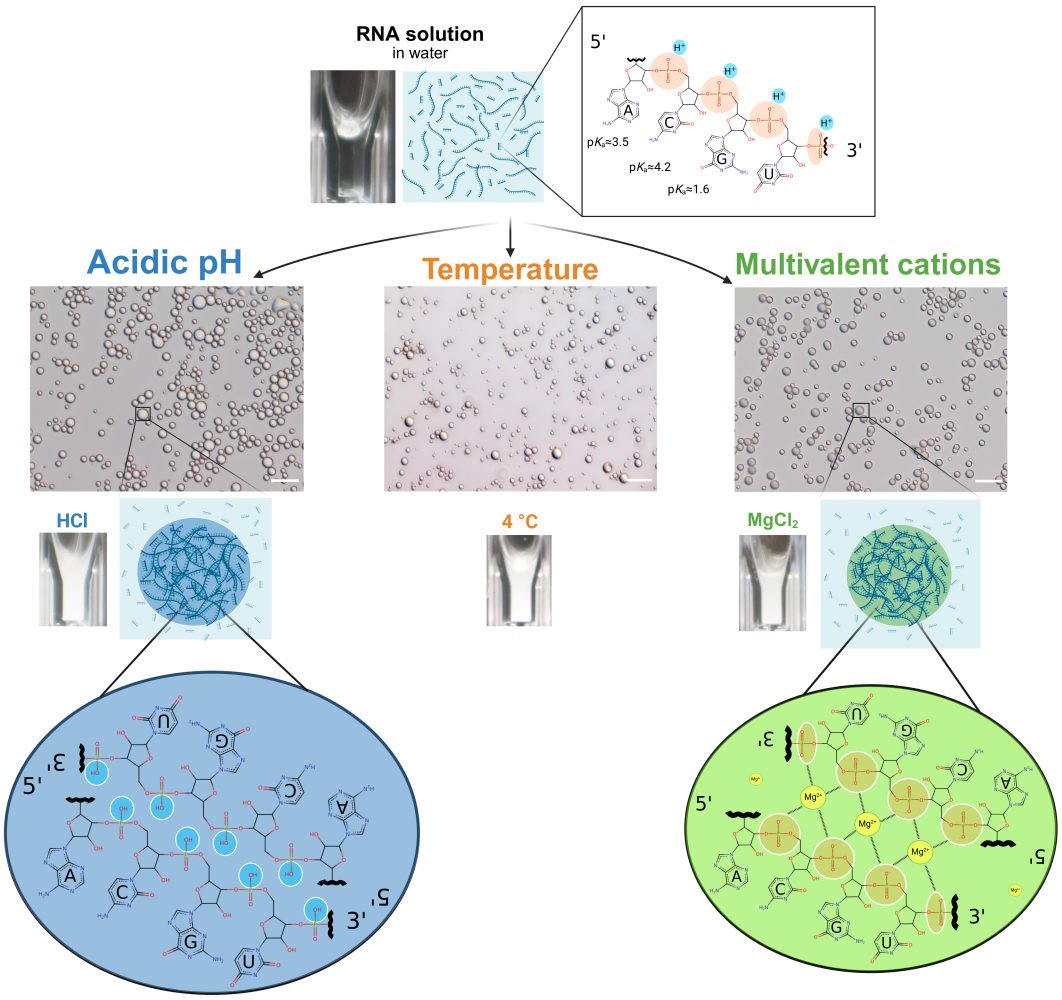

Figure 2: **Overview of conditions inducing RNA phase separation from concentrated solutions**. A near-saturated RNA solution (5-10 g/L at room temperature) forms phase-separated condensates under diverse conditions: decreasing pH with acids (left, blue), lowering temperature (middle), or introducing multivalent cations such as Mg^{2+} (right, green; see also Fig. S2). Microscope images show the resulting RNA condensates under each condition. The molecular mechanisms promoting RNA condensation are illustrated for acidic conditions (protonation of phosphate groups, blue) and multivalent cations (electrostatic interactions with RNA strands, green), both leading to reduced RNA solubility by diminishing backbone charge repulsion.

determined that protonation of the phosphate backbone (the pK_a value trend is indicated with an arrow in Fig. 3d, left) plays a critical role in driving RNA phase separation.

The solubility of RNA is primarily determined by the charge and hydrophilicity of its sugar-phosphate backbone, which is significantly affected by phosphate protonation. This explains why RNA solubility increases dramatically in alkaline conditions: while 16 mg of RNA cannot be fully dissolved in 1 mL of pure water at room temperature, the addition of potassium hydroxide (KOH) enables dissolution of more than 500 mg/mL (Fig. S1a).

Our experimental data (Fig. 3) combined with the present literature suggest a common mechanism underlying these diverse phase separation triggers. Low temperature reduces the solubility of RNA and influences RNA-solvent and RNA-RNA interactions.[48] Strong acids protonate the phosphate backbone, reducing repulsive negative charges between RNA strands. Multivalent ions screen the backbone's negative charges and potentially coordinate different RNA strands via electrostatic interactions[49,50] (Fig. 2, bottom). Thus, reduced RNA solubility (primarily through diminished backbone charge) allows attractive hydrophobic interactions between the nucleobases to drive phase separation.

Since high ion concentrations (>20 mM $MgCl_2$; Fig. 3a) may be unlikely in prebiotic environments with abundant RNA, we investigated whether organic co-solutes could enhance phase separation at low ion concentrations. Indeed, various organic co-solutes (propylene glycol, 1,6-hexanediol, DMSO, and PEG) significantly promote phase separation at low magnesium concentrations (10 mM; Fig. S1c). Relatively modest co-solute concentrations (5%) is enough to enhance phase separation, with increasing concentrations amplifying the effect (Fig. S1c).

RNA condensates produced with 200 mM HCl or $MgCl_2$ had similar volume fractions (1-2%; Fig. 3e), but different RNA concentrations within the condensates. $MgCl_2$-induced condensates contained higher RNA concentrations (approximately 200 g/L vs. 150 g/L for HCl-induced condensates; Fig. 3f), suggesting structural differences between these types of condensates.

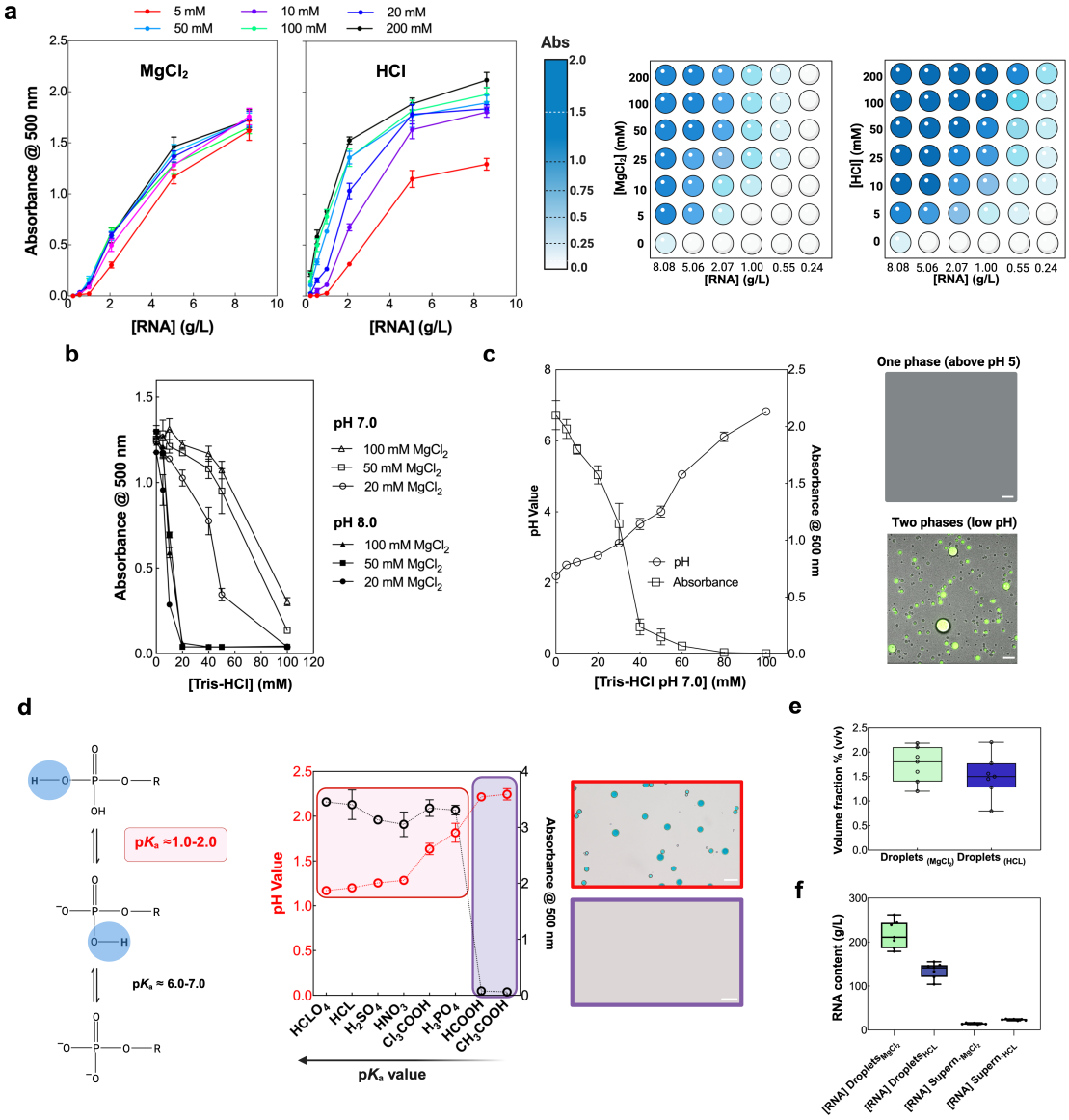

Figure 3: **RNA phase separation mediated by divalent cations and by adding hydrochloric acid**. **a**, Absorbance measurement at 500 nm of RNA used at different concentrations (ranging from 0.237 to 8.089 g/L) in the presence of several $MgCl_2$ and HCl concentrations (ranging from 5 mM to 200 mM). In the presence of low concentrations of HCl (10 mM) RNA undergoes phase separation even at the lowest concentration tested (0.237 g/L). On the other hand, $MgCl_2$ triggers RNA phase separation when 0.5 g/L of RNA are mixed in the presence of at least 25 mM $MgCl_2$ (light blue dots in the heat-map). **b**, RNA phase separation (RNA 5 g/L) measured by monitoring the absorbance at 500 nm in the presence of different $MgCl_2$ concentrations (100, 50 and 20 mM) against different concentrations of Tris-HCl at pH 7.0 (empty symbols) and pH 8.0 (full symbols).

Figure 3 (continued): **c**, RNA phase separation measured through absorbance (empty square and line) correlated to the pH (empty dots and line) using different concentrations of buffer (Tris-HCl pH 7.0). RNA phase separation was obtained by using a fixed $MgCl_2$ concentration (100 mM). **d**, RNA phase separation in the presence of different acids. Schema representing the pK_a values for the protonation states of the phosphate group. Graph reporting the trend of the pH (red line and dots) and absorbance (black line and dots) of RNA (10 g/L concentration) in the presence of different acids with different pK_a (10-20 mM final concentration of all acids have been used). Absorbance (black) and pH (red) points within the pink region indicate RNA phase separation while the violet region indicates no RNA phase separation. **e**, Condensate volume fraction obtained using $MgCl_2$ and HCl 200 mM to trigger RNA phase separation. **f**, RNA content in the condensates and supernatant after separation of the two phases. The RNA condensates in **e** and **f** were prepared using $MgCl_2$ and HCl at 200 mM final concentration.

The remarkable ease with which RNA phase-separates in response to diverse triggers — temperature, pH, multivalent cations, and molecular crowding — highlights its unique capacity for condensate formation, a property not readily observed with other macromolecules. Additionally, RNA condensates selectively enrich longer RNA species over shorter ones (Fig. S1b, Fig. S4, and Fig. S12), likely due to favorable enthalpic interactions from increased valency counterbalanced by lower entropic costs.[51,52]

These properties facilitate phase separation and selective enrichment of longer RNAs, potentially offering a solution to the Flory Length Problem in origin of life scenarios. The rare species of randomly produced longer RNA could be concentrated and compartmentalized within condensates. Assuming the catalytic capacity to polymerize nucleotides,[53] new RNA molecules could have been synthesized within the compartments. This raises the question whether nucleotides and other relevant biomolecules could be enriched in these RNA condensates to enable catalytic activities.

Partitioning of small molecules within RNA condensates

From an origin of life perspective, an important feature of a protocell is its ability to interact with and compartmentalize a wide variety of organic molecules coupled with its ability to catalyze chemical reactions. Guest molecules should have a variety of different physicochemical

characteristics and sizes to enable the complex chemistry essential to form entities capable of sustaining primordial chemical reactions. The enrichment of small molecules is therefore an essential property of any protocell system and has been reported for other systems.[31]

With these premises, we analyzed the partitioning of several organic guest molecules into RNA condensates as reported in Fig. 4 and checked the diffusion of small organic molecules within the condensates (Fig. S5). As expected, small organic molecules (such as rhodamine) can easily enter the droplets and small aromatic fluorophores such as methylene blue, 4,6-diamidino-2-phenylindole (DAPI), resorufin, and SNARF are highly concentrated inside RNA condensates (Fig. S6). In addition, ATP was also enriched within RNA condensates, as was FMN (although to a lower extent) (Fig. 4).

Another important property of protocells is the encapsulation of longer, potentially information-coding biopolymers like nucleic acids. As shown in Fig. S1 the RNA condensates enrich longer species of RNA. RNA condensates prepared from solutions containing short RNA fragments using both $MgCl_2$ and HCl (10 mM) are also enriched by longer labeled nucleic acids like RNA, single-, and double-stranded DNA (Fig. 4 and also for example Fig. S4, Fig. S12).

Several coacervate systems have the drawbacks that encapsulated molecules easily cross the membrane-less droplet boundary and that the coacervate phase quickly coalesces into one phase. The movement of encapsulated species across the boundary of membraneless coacervate droplets and the coalescence of droplets are issues that have so far hampered their use as protocell models.[30,54,55]

The RNA system reported here limits this drawback. The mobility of RNA between the condensate droplets was tested by preparing three different RNA condensate populations with synthetic RNAs carrying different fluorescent labels (Fig. S4a). Although slow fusion events and wetting could be observed, the populations remained distinct for extended periods of time after mixing (Fig. S4b,c). This result demonstrates that RNA can be efficiently compartmentalized within RNA condensates, maintaining (during the limited experimental

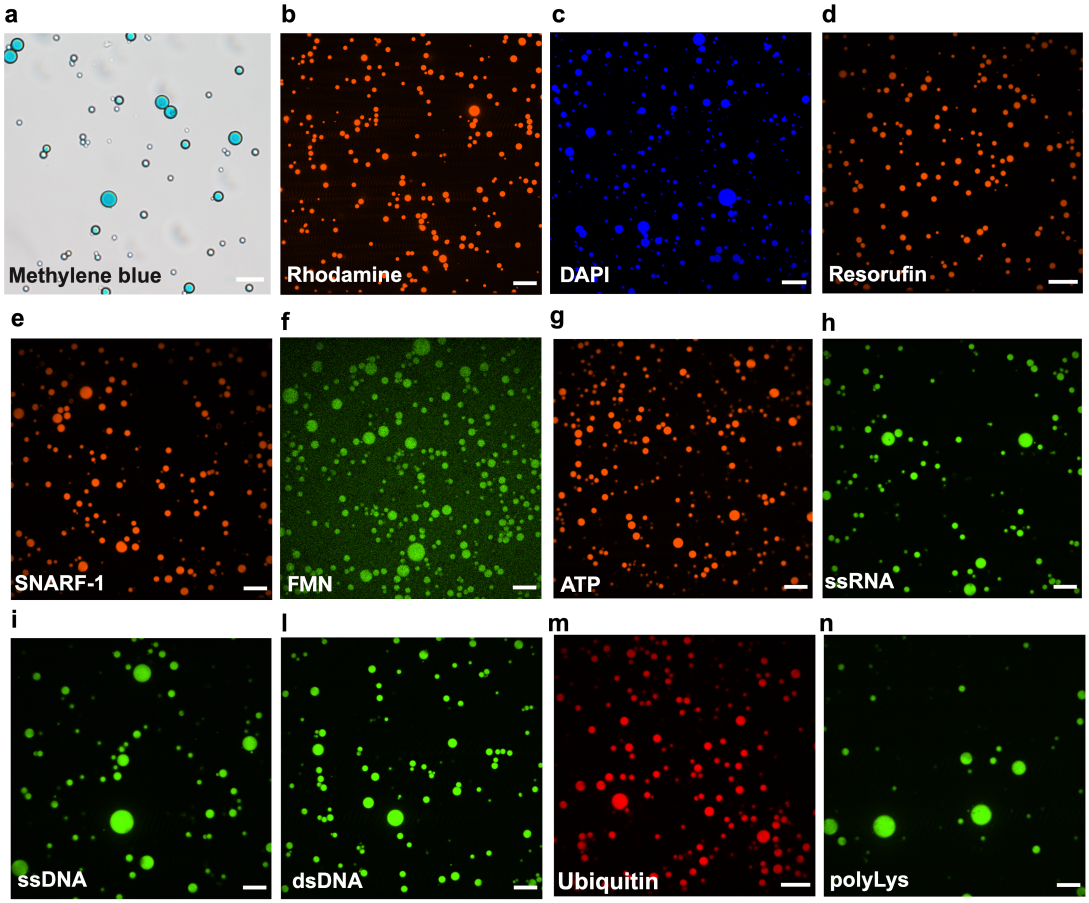

Figure 4: **Partitioning of small organic molecules, nucleic acids and peptides within the RNA phase-separated condensates.** **a**, RNA phase-separated condensates have been obtained by adding 10 mM HCl to 5 g/L RNA in the presence of **a**, methylene blue. **b**, rhodamine 5G. **c**, DAPI. **d**, resorufin. **e**, SNARF™-4F 5-(and-6)-carboxylic acid. **f**, FMN. **g**, ATP visualized using BioTracker ATP-Red Live Cell Dye. **h**, FAM labeled ssRNA. **i**, FAM labeled ssDNA. **l**, FAM labeled dsDNA. **m**, ubiquitin and **n**, FITC labeled polyLys. The concentration of small organic molecules partitioned in the RNA phase-separated condensates was between 200 nM and 20 µM. The same molecules at the same concentration can be partitioned by using 10 mM $MgCl_2$ using 5 g/L RNA. The quantification of the signal within and outside the condensates is reported in Fig. S6.

time) separate genetic identities. Phase-separated RNA thus seems to fulfill some essential requirements for a protocell system[56] that have been difficult to achieve with other phase-separated systems, such as reduced Ostwald ripening and efficient compartmentalization of RNA species required for Darwinian-style evolution.

An important role of RNA in extant biochemistry is the assembly of peptides from amino acids, which supposedly is a remnant of the RNA world.[57] Therefore, we investigated how the RNA phase interacts with amino acids and peptides. Interestingly, RNA condensates partition peptides and small proteins of different length. As reported in Fig. 4, ubiquitin (8.6 KDa, 76 aa) and the longer poly-Lys (15-30 KDa) are enriched within the RNA phase while amino acids are roughly equally distributed between both phases (Fig. S7). Besides interacting with small molecules and peptides, the RNA condensates also partitioned phospholipids, which spontaneously formed sub-structures inside the RNA condensate. Fatty acids (C11 and C12) spontaneously assembled on the condensate surface (Fig. S8) that resemble a primordial layer.

In summary, many different small molecules and even more complex biopolymers partition into RNA condensates. Importantly, longer RNA species and nucleotides are enriched. The enrichment of molecules and the ease of RNA phase separation, without the need for other polymers or components, are promising indications for the potential of RNA condensation in the context of the origin of life. The findings also open the door for investigations into the catalytic potential of RNA condensates as microreactors for chemical reactions.

RNA condensates as prebiotic microreactors: catalytic enhancement of simple chemical reactions

Driven by the enrichment of molecules within RNA condensates, we investigated whether these compartments could catalyze or enhance simple chemical reactions relevant to prebiotic chemistry. Hydrolysis, condensation, and transamination reactions would have been critical for the formation and interconversion of the building blocks necessary for life. Hydrolysis

is fundamental to metabolism and energy transfer in living systems,[33] while condensations allow the formation of complex molecules from simpler precursors. Transamination, the transfer of amino groups between molecules, represents a key process for amino acid synthesis and nitrogen cycling in primitive metabolic networks.[58,59]

We first examined the hydrolysis of para-nitrophenyl acetate (pNPA, Fig. 5a), a widely used substrate for evaluating esterase activity that has been previously employed to study catalysis in compartmentalized systems.[60,61] Under our experimental conditions (pH 2.0 - 2.5), the acid-catalyzed hydrolysis of pNPA is extremely unfavorable: the mechanism requires protonation of the ester carbonyl and water is a particularly weak nucleophile in acidic environments. Our kinetic analysis revealed reaction rates of 2.95×10^{-9} M/s for 5 mM pNPA in RNA condensates, compared to 1.93×10^{-9} M/s in the diluted phase. Although this enhancement is modest, the fact that we observed any acceleration under such unfavorable conditions suggests that RNA condensates may provide alternative reaction pathways, potentially through specific functional groups within the RNA structure serving as general acid-base catalysts or through creating microenvironments with altered local reactivity compared to bulk solution.

More significant effects were observed with the formation of 2,4-dinitrophenylhydrazones (Fig. 5b), a model condensation reaction. Condensation reactions are crucial in prebiotic chemistry for the formation of carbon-carbon and carbon-nitrogen bonds to build complex organic molecules from simple precursors. The reaction of 2,4-dinitrophenylhydrazine (2,4-DNPH, 200 µM) with vanillin or p-anisaldehyde (400 µM) proceeded substantially faster in RNA condensates compared to control conditions. For p-anisaldehyde, we measured a rate constant of $4.46 \pm 0.62 \cdot 10^{-4}\mu M^{-1}min^{-1}$ in RNA condensates, compared to $5.06 \pm 0.46 \cdot 10^{-5}\mu M^{-1}min^{-1}$ in the supernatant phase, representing an 8.8-fold acceleration. Similarly, for vanillin, the rate constant increased from $2.59 \pm 0.34 \cdot 10^{-5}\mu M^{-1}min^{-1}$ in the supernatant to $1.73 \pm 0.30 \cdot 10^{-4}\mu M^{-1}min^{-1}$ in RNA condensates, a 6.6-fold enhancement. The improved reactivity correlates closely with the observed 6-7 fold higher concentration of 2,4-

DNPH within the condensates (Fig. S9d), providing quantitative evidence that molecular partitioning is the primary driver of the catalytic effect in this case (concentration effect).

Perhaps most remarkably, RNA condensates showed robust enhancement of transamination reactions. Glyoxylate was converted to glycine at acidic pH using various amino acids as donors. Glyoxylate is considered an abiotically accessible organic compound and important prebiotic building block linked to protometabolism,[62–64] while glycine, the simplest amino acid, is fundamental for early peptide formation[65] and has been detected in meteorites and prebiotic simulation experiments.[66] The reaction proceeded efficiently at room temperature in the presence of RNA condensates, but less so in the supernatant phase or water (Fig. 5c). Using L-ornithine as the amino donor, the glycine concentration reached approximately 4192.45 µM in the presence of RNA condensates, compared to only about 994.83 µM in the supernatant phase and 482.67 µM in water. The reaction rates showed even more dramatic differences: 107.26 µM/min in the presence of RNA condensates versus just 13.76 µM/min in the supernatant and 9.71 µM/minin water. Similar enhancements were observed using L-lysine (38.01 µM/min in condensates vs. 1.83 µM/min in water) and L-alanine (14.62 µM/min vs. 1.03 µM/min in water) as amino donors.

This transamination reaction is typically unfavorable at acidic pH because the protonation of amino groups reduces their nucleophilicity and impedes the formation of imine intermediate essential for the reaction mechanism (see SI for detailed discussion). Despite these challenging conditions, RNA condensates dramatically enhance the amination of glyoxylate. In fact, the reaction did not proceed efficiently in water or in the diluted phase. In a setup with high RNA concentrations but without triggering phase separation (without condensate formation by addition of $MgCl_2$ 100 mM) the reaction was also inefficient (data not shown). This demonstrates that RNA condensates function as efficient microreactors for such transamination reactions by combining selective enrichment with intrinsic catalytic capabilities. The synergistic effects of RNA structure, magnesium ions, and amino acid properties create an environment that significantly enhances reaction rates and yields,

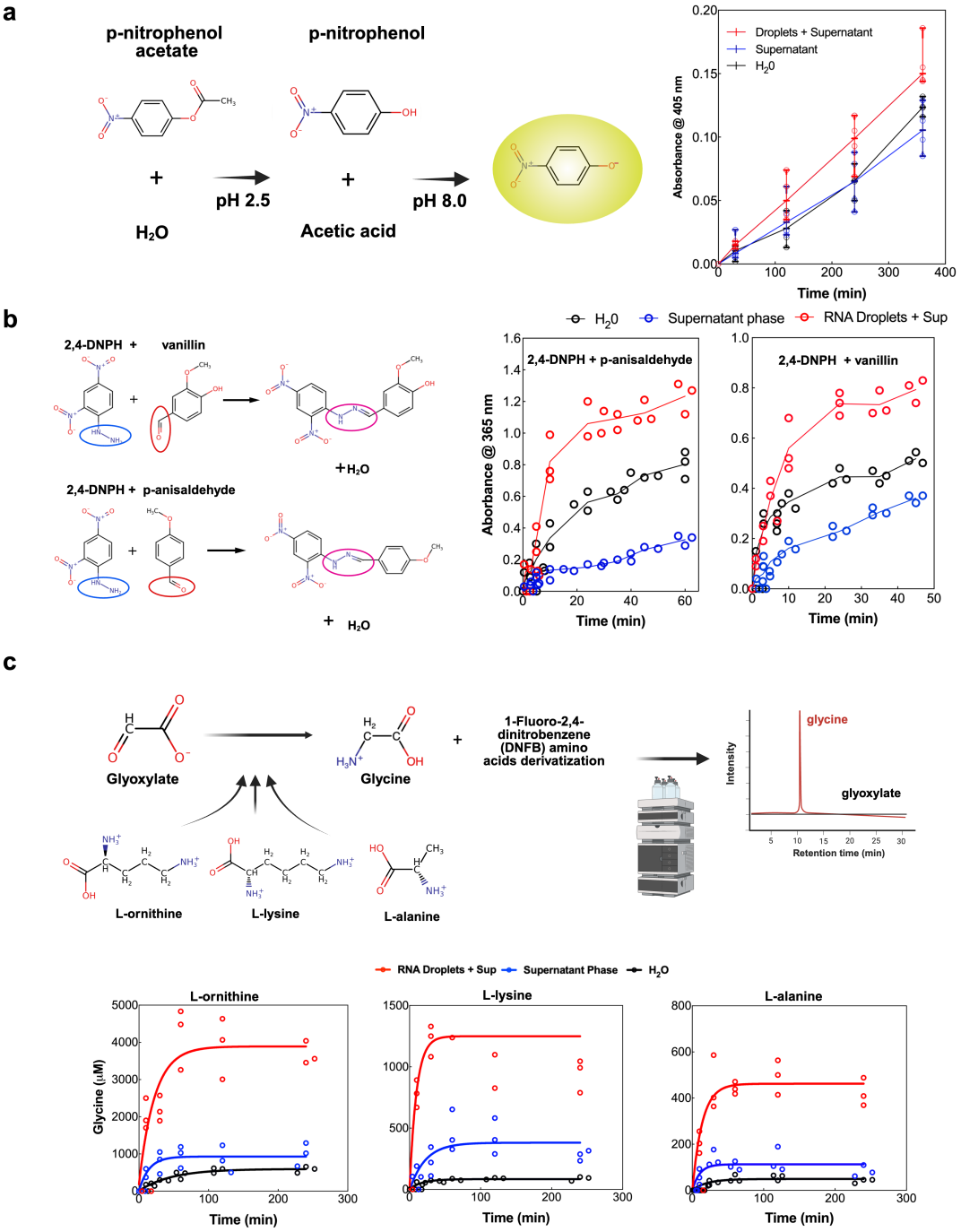

Figure 5: **Small organic molecule catalysis within the phase-separated RNA condensates. a**, Enhanced acid hydrolysis of 10 mM p-nitrophenol-acetate (pNPA) in the RNA condensates (red dots and line) resulting in the two products, p-nitrophenol (yellow at neutral and basic pH) and acetate, compared to the supernatant phase (blue dots and line) and only water (black dots and line) in the presence of 100 mM $MgCl_2$. Fig. S10 shows the hydrolysis of pNPA at two different concentrations, 2 mM and 0.5 mM as well as the schema of the procedure used to set up the experiments.

Figure 5 (continued): **b**, Addition reaction formation rates between 2,4-dinitrophenylhydrazine and aldehydes: p-anisaldehyde to form p-anisaldehyde,2,4-dinitrophenylhydrazone (left) and vanillin to form vanillin,2,4-dinitrophenylhydrazone (right). 2,4-dinitrophenylhydrazine was used at a fixed concentration of 200 µM and the aldehydes at 400 µM, with 100 mM $MgCl_2$ to trigger phase separation. The raw data and absorbance graphs of the reactions are reported in Fig. S9. **c**, HPLC profiles of glycine production within RNA condensates (red dots and line) compared to the diluted phase (blue) and water (black). The amino donors used were L-ornithine, L-lysine and L-alanine at a fixed concentration of 10 mM. The alpha-ketoacid used was glyoxylate at a fixed concentration of 20 mM. After incubation and derivatization with 1-fluoro-2,4-dinitrobenzene (see Materials and Methods), the amino acids were detected using HPLC. The HPLC chromatograms related to glycine production and the amino acid calibration curves are reported in Fig. S7. The experiments performed in water contained the same concentrations of $MgCl_2$ (100 mM) and the same acidic pH (adjusted with HCl) as the condensates and supernatant samples.

particularly under conditions that would otherwise be unfavorable. These findings provide valuable insights into potential mechanisms of prebiotic chemical evolution and highlight the remarkable catalytic potential of RNA-based compartmentalization (Fig. S7c).

Folding and catalytic activity of macromolecules within RNA condensates

We have shown that RNA solutions easily phase-separate under a variety of conditions and that the phase-separated RNA condensates enrich longer RNA species and different small organic molecules, thereby enhancing different organic reactions such as hydrolysis, addition reactions, and transamination. An additional challenge for these condensates to be a viable protocell system is their capacity to support specialized catalytic activity of biopolymers.

On first sight, the conditions inside the condensed RNA phase seem unfavorable for biopolymer catalysis. Condensates form at high RNA concentrations and low pH. However, most enzymes and ribozymes are not active at pH below 4. Further, at high nucleic acid concentrations non-specific base pairing could disrupt proper folding of ribozymes and essential ions (e.g. magnesium) could also be sequestered by other RNAs. Therefore, a proof of bio-

logically relevant catalytic activity of ribozymes and protein enzymes inside the condensed RNA phase is necessary.

We tried to demonstrate proper folding of RNA and protein within the condensates using fluorescent RNA aptamers spinach[67] and pepper[68] as well as labeled BSA and GFP. The RNA aptamers spinach and pepper fold into a specific three-dimensional structure that selectively bind an organic molecule (their ligand). This complex of aptamer and ligand shows strong fluorescence while the aptamer and ligand alone are not fluorescent.[67,68] The fluorescence signal therefore provides a convenient read-out for correct folding of the aptamer and the molecular recognition (binding) of its ligand.

Although it was impossible to demonstrate RNA folding using fluorescent RNA aptamers due to unspecific activation of the dyes in the RNA condensates (data not shown), fluorescently labeled BSA and GFP could be observed within the RNA condensates, indicating partition of the proteins into the condensates Fig. 6a. Furthermore, GFP fluorescence data indicate that protein folding is maintained within the RNA condensates, because GFP loses its fluorescence upon unfolding.[69] On the basis of the protein partitioning data, we decided to evaluate if protein catalysis was possible inside the condensates. For this purpose, we used Oxalate decarboxylase (OxDC) from *Bacillus subtilis*. OxDC is a homohexamer (a dimer of trimers) of 264 kDa which belongs to the cupin superfamily and requires Mn^{2+} and O_2 to catalyze the conversion of oxalate to formate and CO_2. Notably, the pH optimum of this enzyme is at pH 4.2 but with a wide range of activity.[70] As reported in Fig. 6a-b, OxDC partitioned into RNA condensates and also showed activity inside. Although the enzymatic activity measured within the condensates (11 ± 2 s^{-1}) is low compared to that obtained in diluted conditions in buffer at pH 4.2 (74 ± 6 s^{-1}) using 10 mM oxalate,[71] it confirms that enzymes can be active inside RNA condensates. Notably, the product of the enzymatic reaction (formate) dissolves the droplets (Fig. 6b and Fig. S11).

Although the results obtained with proteins are promising, for the system to be a relevant protocell model inside the RNA world framework, it needs to be able to support nucleic acid-

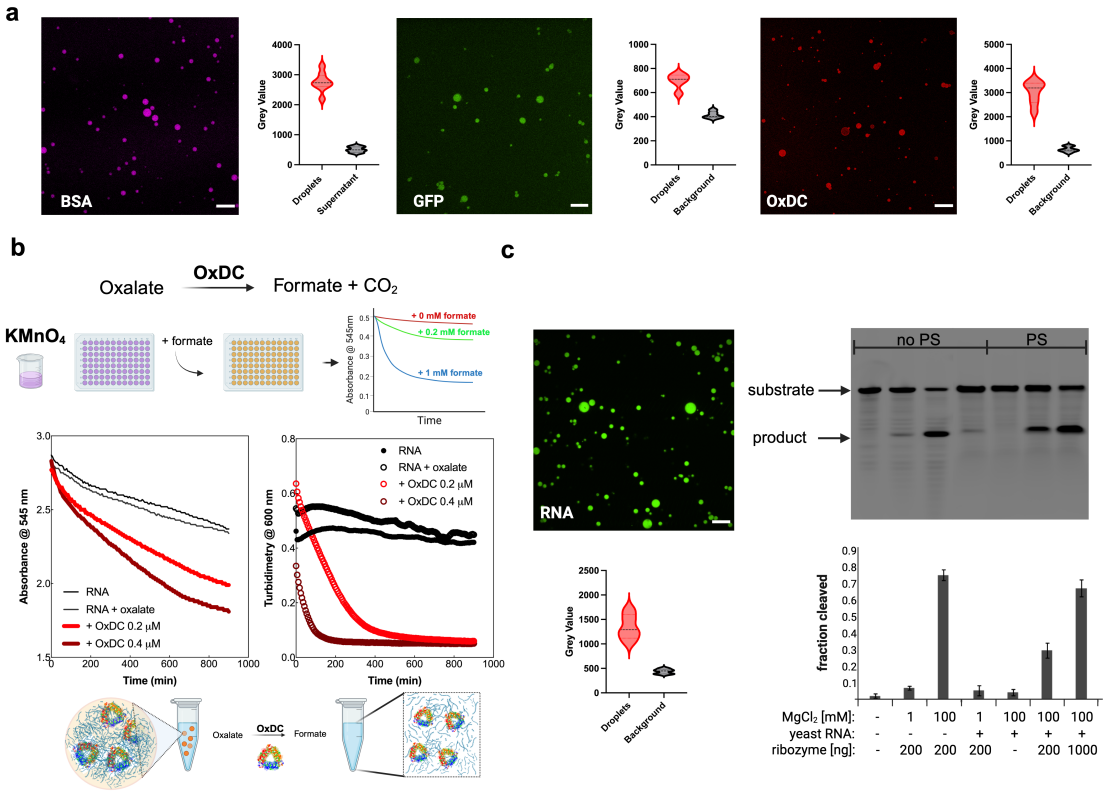

Figure 6: **RNA condensates can accommodate catalysis mediated by macromolecules. a**, Partitioning of proteins within the phase-separated condensates. In detail, 10 µM BSA labeled with Alexa Fluor 647 nm, 20 µM GFP and 5 µM OxDC have been partitioned within the condensates prepared using Tris-HCL 32 mM pH 7.5 in the presence of (3-3.5 g/L RNA and 100 mM $MgCl_2$). The proteins have been added just before $MgCl_2$, which triggers phase separation. The fluorescence intensity value (grey-scale value) of the signal within and outside the condensates is also shown. **b**, Schema of the assay used to measure the OxDC activity within the RNA condensates. To monitor the activity, the decrease of the potassium permanganate signal (545 nm) was followed. Permanganate reacts with the formate produced by OxDC.[71] Left: OxDc activity (light and dark red line) measured using two different protein concentration 0.2 µM and 0.4 µM in the presence of 10 mM oxalate. In black are reported the decrease of the signal in the presence of only RNA and RNA and the substrate oxalate 10 mM final concentration. Right: turbidimetry measurements at 600 nm during the reaction catalyzed by OxDC. The decreasing signal at 600 nm corresponds to the disappearance of condensate caused by formate production.

Figure 6 (continued): **c** Ribozyme activity within the RNA condensates after 30 minutes. Left: Microscopic picture showing that the FAM-labeled ribozyme substrate is located inside the RNA condensates and quantification of the fluorescence signal in condensates compared to background. Right, top: Representative PAGE gel. Visible is the FAM-labeled ribozyme substrate and the label-carrying cleavage product of the ribozyme reaction. Right, bottom: fraction of the substrate cleaved as averages with standard deviation derived from gel pictures of at least three experiments. Conditions with and without phase separation (PS) are indicated. From left to right: The substrate is stable buffer (lane 1). In the presence of ribozyme at pH ≈ 3, weak cleavage (around 10%) is observed at 1 mM (lane 2) and around 75% cleavage at 100 mM $MgCl_2$ (lane 3). In the presence of 5 g/L yeast RNA, 1 mM $MgCl_2$ does not cause phase separation and ribozyme cleavage rate is not influenced (lane 4; compared to lane 2 without yeast RNA). Phase separation of yeast RNA is triggered at 100 mM $MgCl_2$, but this does not impact the stability of the substrate in the absence of ribozyme (lane 5). In the presence of ribozyme, phase separation causes a drop in cleavage to around 30% (lane 6). Ribozyme is therefore still active inside the condensates but with lowered activity compared to bulk. The cleavage depends on the ribozyme dose with a 5-fold increase in ribozyme achieving nearly 70% fraction cleaved (lane 7).

based catalysis. Therefore, the catalytic activity of nucleic acids was investigated using a hammerhead ribozyme.[72] The ribozyme partitioned well into the RNA phase as shown on denaturing gels after separating condensates and supernatant by centrifugation (Fig. S12). The hammerhead ribozyme showed activity in RNA condensates formed from yeast RNA at 100 mM $MgCl_2$ (Fig. 6c) or when adding PEG8000 at high concentrations (around 20%; data not shown). Although the activity of the ribozyme was less than 50% compared to the dilute condition without yeast RNA, the catalytic activity of the hammerhead ribozyme obtained inside the RNA condensates is promising.

This ribozyme is not adapted to the conditions used (low pH and high RNA crowding). Despite the many issues that could interfere with ribozyme catalysis, the activity observed was robust and dependent on the ribozyme concentration (Fig. 6c). A 5-fold increase in ribozyme concentration increased substrate cleavage to a level similar to that observed in dilute conditions. This shows that ribozymes can function inside the RNA condensates and we propose that in vitro selection of ribozymes under these conditions could yield ribozymes with good activity. The high RNA concentrations inside the condensates (>100 g/L) together with their catalytic capabilities and the enrichment of other molecules might be particularly

favorable for the evolution of ligase or replicase ribozymes that could start evolutionary processes in the RNA world.

Conclusion

RNA might have played a pivotal role in the emergence of life by performing multiple critical functions: storing genetic information, catalyzing biochemical reactions, and acting as a template for replication. Our findings demonstrate that RNA readily phase-separates under acidic conditions without requiring other biopolymers or small molecules. However, the resulting RNA condensates selectively enrich small molecules, peptides and more complex macromolecules such as functional ribozymes and enzymes.

Importantly, RNA condensates enhance biochemical reactions. They do so through two different mechanisms: First, through a concentration effect, these condensates create microenvironments where substrates and potential reaction partners are brought into close proximity, significantly increasing the probability of productive molecular interactions (addition reaction). Second, through an inherent catalytic effect, the RNA itself possesses intrinsic catalytic properties that can accelerate specific biochemical reactions independently of the concentration advantages (transamination reaction). These two distinct effects — local concentration of substrates and intrinsic catalytic properties — enable RNA condensates to enhance fundamental biochemical reactions even in the absence of dedicated catalysts. The RNA condensates can potentially facilitate other reactions that were not investigated.

Although our system does not directly address the abiotic origins of RNA, it provides substantive support for the possibility of the emergence and evolution of an early RNA world under acidic conditions. Geological evidence suggests that early Earth's surface environments could have been moderately acidic, providing favorable conditions for RNA phase separation.[13] This scenario would address the issue of RNA stability, supporting the hypothesis that the RNA world evolved at acidic pH.[73] Acidic conditions further facilitate RNA-RNA strand separation,[74] essential for replication processes. A legitimate concern re-

lates to RNA functionality under acidic conditions; however, hammerhead ribozyme activity has been demonstrated at pH values as low as 3,[75] indicating that low pH does not necessarily impede RNA folding and function. Furthermore, RNA phase separation can be triggered by various metal ions that would likely be sequestered within RNA condensates where they could enhance catalysis.

The stable encapsulation of genetic material within the condensates indicates a plausible mechanism for maintaining genetic information within discrete catalytically active compartments, a necessary prerequisite for the evolution of more complex protocells. Such compartmentalization could potentially have facilitated the gradual accumulation of active RNA sequences, thereby contributing to the molecular selection of condensates with enhanced functionality or stability. As such systems evolved, they could have developed and profited from interactions with other environmentally available molecules, for example fatty acids,[76] which could have driven the development of increasingly complex boundary structures. These interactions may represent a coherent pathway toward the eventual emergence of membrane-bound protocells from initially membrane-free RNA condensates.

Materials and Methods

Materials

RNA from yeast was from Roche 10109223001 or Fujifilm-Wako 4987481380561. RNA from torula yeast was purchased from Merck (R6625). NTP stock solutions (100 mM) were obtained from NEB. RNAse free water, propylene glycol, 1,6-hexanediol, dimethylsulfoxide (DMSO), and polyethylene glycol 200 (PEG200), HCl, sodium chloride, urea were purchased from Nacalai Tesque. Tris-HCl (varying pH from 7 to 9) and $MgCl_2$ solutions were ordered as 1 M stock solutions from Nippon Gene. The different salts tested were calcium chloride (Fujifilm Wako Pure), manganese sulfate (33341 Alfa Aesar), iron II sulfate (14498 Alfa Aesar), cobalt II chloride (255599 Merck), zinc chloride (208086 Merck), copper chloride (751944

Merck), sodium molybdate (243655 Merck), iron III chloride (F2877 Honeywell). PEG 200 was purchased from Tokyo Chemical Industry (TCI). L-Amino acids (L-alanine (A7627), L-ornithine (O2375), L-lysine (L5501), L-norvaline (D7627) and glycine (G7126)), DNFB (D1529), 2,4-dinitrophenylhydrazine (DNPH, D199303), p-anisaldehyde (A88107), vanillin (V1104), ubiquitin from bovin erythrocytes (U6253), glyoxylate sodium salt (G4502), pNPA (N8130), pNP (241326), Rhodamine-B (R6626), resorufin sodium salt (R3257) methylene blue (M9140), poly-L-lysine FITC labeled (P3543), DAPI (D9542), bovine serum albumin (BSA, A7638), β-Nicotinamide adenine dinucleotide, reduced disodium salt hydrate (NADH) (N8129), Pyruvate (P8524), Pyridoxal 5'-Phosphate (PLP), rabbit muscle L-lactate dehydrogenase and isopropyl-β-D-thiogalactoside were purchased from Merck (Germany). Fatty acids (D3835, D3821 and D3861), phospholipids (β-BODIPY™ FL C12-HPC (2-(4,4-difluoro-5,7-dimethyl- 4-bora- 3a,4a-diaza-s-indacene- 3-dodecanoyl)- 1-hexadecanoyl-sn-glycero- 3-phosphocholine)(D3792), SNARF™-4F 5-(and-6)-carboxylic acid, acetoxymethyl ester, acetate (S23921), Alexa Fluor 647 Microscale Protein Labeling Kit (A30009) were purchased from Thermo Fisher Scientific.

BSA, OxDC and ubiquitin labeling

BSA, OxDC and uniquitin from bovin liver erythrocytes were tagged using Alexa Fluor 647 Microscale Protein Labeling Kit, using the manufacturer's protocol but repeating the dialysis step three times to remove the free dye in the protein solution as reported.[40]

Preparation of RNA solutions

RNA solution was prepared by adding 200 mg of yeast RNA in 15 mL of DNAse/RNAse free water in 15 mL centrifuge tubes. The mixture was heated to 50 °C and vigorously shaken to dissolve as much RNA as possible. Subsequently, the solution was cooled to room temperature for at least 30 minutes so that the RNA partially precipitated. The saturated mixture obtained was then centrifuged at 10,000 g for 10 minutes at room temperature.

The supernatant was transferred to a new tube and used immediately or frozen at -20 °C. The frozen stocks were thawed at 50 °C and vigorously shaken from time to time until all precipitated was dissolved; thawed stock solution was cooled to room temperature before use. RNA concentrations were quantified by NanoDrop or by using MultiSkan SkyHigh Microplate reader (Thermo Fisher) using the microdrop Duo Plate. The RNA solution after resuspension in water has been diluted and read at 260 nm in triplicate every time and before use.

Denaturing PAGE

Denaturing PAGE was performed following standard procedure using 8 M urea PAGE gels. Shortly, 15% acrylamide gels containing 8 M urea were prepared from 40% pre-mixed stock of acrylamide/bis-acrylamide solution (40% acrylamide/Bis Mixed Solution (19:1), Nacalai 06140-45). RNA samples were loaded after resuspension and heat denaturation (2 min, 95 °C, then storage on ice) in TBE-Urea Sample Buffer / RNA loading dye (Novex) and run in TBE at 250 V for 50 minutes. Labeled RNA was detected directly while unlabeled RNA was stained with 1x SybrGold (Invitrogen) in 40 ml 1x TBE. Pictures were acquired using the Typhoon FLA 7000 (GE).

RNA phase separation

RNA phase separation has been triggered using RNA solutions prepared as described, both using stock solution or by diluting the RNA stock solution in water on in Tris-HCl buffer. For example, storing the solutions at lower temperature (for example around 0 °C on ice), adding different salts (such as $MgCl_2$, $CaCl_2$, $MnSO_4$, $ZnCl_2$, $CoCl_2$, $FeSO_4$, $FeCl_3$, Na_2MoO_4 prepared as 1 M stock solutions in water), strong acids (hydrochloric acid, sulfuric acid, trichloroacetic acid and perchloric acid) caused RNA to phase-separate (used at different concentrations). The exact conditions are described in the manuscript. To estimate the volume fraction, condensates from a total of 10 mL were left to settle over night in 15 mL

centrifuge tubes. The tubes were then flicked carefully and left for another 30 minutes to allow condensates from the side of the tube to settle to the bottom. The supernatant was carefully removed before the volume of the condensate phase was estimated by pipette. For the estimation of RNA content, the condensates were resuspended in 15 mL water with heating to 50 °C before measuring with absorption at 260 nm. Resuspension as well as volume estimation values provided are the best possible estimates.

Effect of co-solutes

To evaluate the effect on RNA phase separation, co-solutes were added to 3.75 g/L RNA with 10 mM $MgCl_2$ in a 96-well plate at the concentrations indicated. The samples were mixed by shaking by hand and the degree of phase separation was quantified by measuring absorbance at 500 nm using a Tecan Pro plate reader.

Confocal Microscopy

Partitioning of small organic molecules The fluorescence images related to the partitioning of small molecules were acquired and analyzed using a Spinning Disk Confocal (Nikon, Andor CSU) microscope with ×40 or ×63 oil immersion lens (University of Perugia). Fluorescence images related to the partitioning of short chain fatty acids, phospholipids and populations experiments were acquired by using and analyzed using a FluoView FV1200 (Olympus) confocal laser scanning microscope (University of Okayama). Confocal images were acquired for more than 5 independent experiments with similar results. The images collected were analyzed using ImageJ.

Partitioning of fatty acids and phospholipid like molecules RNA condensates were prepared as previously described using a saturated RNA solution. Phospholipid (β-BODIPY C12-HPC, Hexadecanoyl-sn-Glycero-3-Phosphocoline) or short chain fatty acids (we tried both C11 undecylenic acid and C12 dodecanoic acid) were added 5-10 µM after RNA condensate formation with 10 g/L RNA in the presence of 100 mM $MgCl_2$ or HCl at

25 °C. After few minutes, around 30 uL were placed on a glass slide along with a cover slip. The experiments last for 2-3 hours.

RNA condensate populations experiments RNA condensates were prepared using a saturated RNA solution (7 - 10 g/L) by adding 100 mM HCl or 100 mM $MgCl_2$. Before triggering phase separation, fluorescently labeled (FAM, Cy3 and Cy5) ssRNA and ssDNA were added to the RNA solution at the final concentration of 750 nM. In detail, the following 20 nt sequences for ssRNA (5'-/56-FAM/AAGCUUGGUCAGGCUUGUAC-3' and 5'-/5Cy5/AAGCUUGGUCAGGCUUGUAC-3') and ssDNA (5'-/56-FAM/AAGCTTGGTCAGGCTTGTAC-3' and 5'-/5Cy3/AAGCTTGGTCAGGCTTGTAC-3') were used. dsDNA was 5'-/56-FAM/AGGAGAGGA 3' and its unmodified complement (5'-AGGATCTCTTCTCTCTCCTCTCCT-3') ordered as separate oligos from IDT and annealed at 10 µM in 50 mM Tris-HCl (pH 8) with 100 mM NaCl (98 °C, 2 minutes and ramping to 37 °C at 0.1 °C per second). Different populations (with or without the addition of a single fluorescently labeled ssRNA or ssDNA) were prepared in separate glass tubes (10 mL final volume). After 2 -3 hours of incubation in the dark at 25 °C the condensates were gently resuspended by pipetting and mixed together in another microcentrifuge tube. After 5 minutes, around 30 µL of mixed solution containing two populations was placed on the glass slide along with a cover slip for visual analysis.

Small organic molecule catalysis within RNA condensates

Addition formation Fresh stock solutions of 2,4-DNPH (116 mM) and aldehydes (300 mM) were prepared in water under acidic condition. Addition reaction between 2,4-DNPH (200 µM) and the aldehydes (p-anisaldehyde and vanillin, final concentration 400 µM) were performed by preparing the condensates using 5 g/L RNA, at 25 °C, using 100 mM $MgCl_2$ to trigger phase separation. Please note that the addition reaction using RNA condensates prepared with strong acids such as HCl leads to a too fast reaction under this experimental condition. The formation of C-N bonds was monitored by recording the absorbance spectra from 240 to 800 nm in a final volume of 200 µL using a MultiSkan SkyHigh microplate

reader with a 96-well UV-transparent plate. The reaction was monitored under three different conditions: in water, condensate, and supernatant phase. The experiments using the supernatant phase were performed by preparing the condensates as reported above in this section. The solution was then centrifuged for 30 minutes at 16000 g for 30 minutes. The supernatant phase has been separated from the condensate phase and used for the experiments. Since 2,4-DNPH has been reported to interact with protein and nucleic acids, we checked the stability of the 2,4-DNPH signal over time (total time of 60 minutes) in the presence of RNA. Within 60 minutes, the absence of non-specific DNPH signal between 2,4-DNPH and RNA was recorded (although after a few hours it is possible to measure a change in the maximum and intensity of the absorbance peak, indicating interactions between RNA and the hydrazinic compound; Fig. S9c). At this point, we set up the experiment as follows: first, we added RNA 5 g/L, then 2,4-DNPHZ (200 µM) and immediately after aldehydes (400 µM) with $MgCl_2$ 100 mM at 25 °C. In the water samples, pH was adjusted using HCl to match the pH of the RNA condensate and supernatant. The spectra were recorded every 2-5 minutes and the signal reported in the kinetic analysis is the decrease in the absorbance of the peak related to 2,4-DNPHZ.

pNPA hydrolysis Fresh stock solution of pNPA (200 mM) were prepared in DMSO 100% and pNPA hydrolysis was evaluated at three different concentrations (5 mM) and (2 mM) in 1 mL of total solution at 25 °C in water, condensates, and supernatant. Acid hydrolysis of pNPA is slower than that at neutral or basic pH. In addition, the solubility of pNPA is limited. For this reason, we used a total RNA concentration equal to 5 g/L to prepare the condensate phase and the supernatant in the presence of 100 mM $MgCl_2$ and conducted the experiments for longer times (around 360 minutes). The same experiment was performed using condensates prepared by adding different HCl concentrations (decreasing the pH further by adding acid increases the reaction rate related to pNPA hydrolysis). The detection of pNP under acidic conditions is through the monitoring of a band around 320 nm which is completely covered by the RNA signal in our samples and has a weak absorbance

signal (protonated form). For this reason, we decided to monitor the signal of the formed pNP at pH 8.0 which is completely deprotonated. As reported in Fig. S10 we have used KP 200 mM pH 8.0 as buffer to convert pNP in the deprotonated form. Briefly, 50 µL of the reaction mix under acidic conditions have been placed on a 96-well plate along with 150 µL of KP 200 mM pH 8.0 at each time point and immediately read at 405 nm using the MultiSkan SkyHigh microplate reader.

Glycine formation The RNA condensates have been prepared by using 100 mM $MgCl_2$ in the presence of 7.5 g/L RNA. All components of the reaction mixture have been added before $MgCl_2$ which triggers the condensation of RNA. In detail, we used a final concentration of 20 mM for glyoxylate, and 10 mM for l-amino acids with a multichannel pipette to start the reaction at the same time in a final volume of 1 mL under agitation (360 minutes total experimental time). The reaction has been performed at 25 °C and at different time points we have withdrawn 2.5-10 µL and placed in 50 µL borate buffer 0.2 M with 100 µM L-norvaline and then derivatized as described in the supporting information **"Derivatization of glycine and other amino acids coupled with HPLC analysis"**. The experiments using the supernatant phase were performed by preparing the condensates as reported above in this section. The RNA condensate solution was then centrifuged for 30 minutes at 16000 g for 30 minutes. The supernatant phase has been separated from the condensate phase and used for the experiments.

Enzymatic reaction within RNA condensates

Cystalysin activity assay Cystalysin from *Treponema denticola* is a pyridoxal 5-phosphate (PLP)-dependent enzyme that catalyses the α,β-elimination of β-chloroalanine to pyruvate, ammonia and HCl. Since this enzyme produces HCl, it can trigger phase separation of RNA by lowering the pH of the entire water solution. Cystalysin has been expressed and purify as previously described.[77] The activity of cystalysin in the presence of RNA was checked by monitoring the decreasing in pH and the pyruvate formation by using LDH coupled assay as

previously reported.[78] Briefly, before to start the experiments showed in the Fig. S13, we have verified the stability and the activity of the protein in water at pH 5.5 in the presence of RNA and $MgCl_2$ at different concentrations (from 5 mM to 100 mM at 25 °C) (data not shown). Pyruvate formation during the reaction of cystalysin with β-chloroalanine was assayed by coupling the pyruvate produced to the NADH-dependent lactate dehydrogenase-catalyzed reaction. The assays were performed at 25 °C on has been measured by using a MultiSkan SkyHigh microplate reader and UV-transparent 96-well plate. A typical reaction mixture contained 1 mM β-Cl-alanine, 300 µM NADH, 1-5 µM lactic acid dehydrogenase in water in the presence of RNA 400 ng/µL, in a final volume of 200 µL. The reaction was initiated by addition of several concentrations of cystalysin 0.5-2 µM. A molar extinction coefficient of $\varepsilon_{340} = 6220\,\mathrm{M^{-1}cm^{-1}}$ for NADH was used. Determination of the kinetic parameters for the reactions catalyzed by cystalysin was performed by measuring the initial velocities by the assay described above.

OxDC activity assay OxDc wild type has been expressed and purified as reported here.[71] The activity of the enzyme within the condensates has been measured by detecting the product formate using potassium permanganate. Potassium permanganate is a chemiluminescent reagent that is often used to detect organic molecules, and have been using to detect formate.[71] The measurements were initially setup in the presence of different formate concentrations and at a fixed potassium permanganate concentration of 1 mM. The better results have been obtained (as previously reported here[71]) using the variation of the signal at 545 nm and the latter conditions have been used to detect formate produced by the enzymatic reaction of OxDC within the RNA condensates and in the supernatant. The RNA condensates have been prepared in Tris-HCl 32 mM pH 7.5 by mixing 3.7 g/L of RNA in the presence of OxDC 0.2 µM and 0.4 µM with MgCl2 50 mM. The oxalate concentration used in the assay was 10 mM and the reaction temperature was 25 °C. The reaction has been stopped by the addition of 25 µL of the reaction mix to 175 µL of potassium phosphate buffer 100 mM pH 8.0 containing 1.75 mM potassium permanganate (final concentration) in

a total volume of 200 µL and the absorbance at 545 nm of the first 5-10 minutes has been measured by using MultiSkan SkyHigh microplate reader set at 25 °C. The data have been analysed using GraphPad Prism 10.4.1 (GraphPad Software, Boston, Massachusetts USA, www.graphpad.com).

Ribozyme activity

We used a hammerhead ribozyme that had been shown to be active inside coacervate samples.[72] The substrate including a polyA spacer (FAM-aaaaaaaaaaaaaGGCAUCCUGGAUUCCACUCGCC) was ordered as solid-phase synthesized RNA from FASMAC. DNA template encoding the hammerhead ribozyme was prepared by annealing the synthetic DNA oligos (Eurofins) SaH753 TAATACGACTCACTATAGGGCGAGGTACATCCAGCTGACGAGTCCCAAATAG-GACGAAATGCC and SaH754 GGCATTTCGTCCTATTTGGGACTCGTCAGCTGGAT-GTACCTCGCCCTATAGTGAGTCGTATTA to each-other (98 °C for 2 minutes and ramping to 37 °C at 0.1 °C per second using 10 µM oligo each, 100 mM $MgCl_2$, and 100 mM NaCl). RNA was generated using ScriptMAX Thermo T7 Transcription Kit (TOYOBO) according to the manufacturers instruction using 1 µL of the annealed oligos as the template. After a DNA digest (DNase I, Takara), the ribozyme RNA was silica column-purified using the RNA Clean and Concentrator-5 (Zymo) and eluted in RNA-grade water. The concentration and purity were determined by Nanodrop. Reactions were set up in using 50 mM Tris-HCl (pH 3 in the absence of yeast RNA or pH 7 in the presence of yeast RNA), 2.5 mM KCl, 0.2 µM substrate as well as $MgCl_2$, yeast RNA, and ribozyme in amounts indicated. Reactions took place at 37 °C for 30 minutes. The reactions were either precipitated with ethanol and sodium acetate (in cases without phase separation) or separated into supernatant and condensate phase by centrifugation at 18 000 g for 5 minutes. Both the condensate phase and precipitated reactions were resuspended in TBE-Urea Sample Buffer / RNA loading dye (Novex) at 95 °C for 2 minutes, cooled on ice, and completely loaded onto a 15% TBE-polyacrylamide gel containing 8 M urea. Ribozyme activity was estimated after PAGE by

quantifying the cleaved bands relative to the uncleaved substrate band on pictures taken with the Typhoon FLA 7000 (GE) using ImageJ.

Statistics and reproducibility

The experimental data reported in this manuscript were performed at least in triplicate. The error bars shown along the manuscript represent the SD. Data were analyzed with GraphPad Prism 10.4.1 (GraphPad Software, Boston, Massachusetts USA, www.graphpad.com). The authors will provide all the necessary data to evaluate the manuscript.

Acknowledgement

The research was supported by the Okinawa Institute of Science and Technology Graduate University (OIST) with subsidy funding to Y.Y.. M.D. thanks the Japan Society for the Promotion of Science (JSPS) for the Kakenhi Early Career Scientist N. 22K15065, and R.N. acknowledges support from MEXT's 'Initiative for Realizing Diversity in the Research Environment. The authors thank Prof. Paola Laurino, Mr. Alessandro Bevilacqua, Prof. Claudio Constantini, Prof. Davide Chiasserini and Dr. Franco Cardone for critical reading. The authors thank Yoshiteru Iinuma from the Instrumental Analysis Support at OIST for performing the trace element analysis. The images were prepared using Biorender.com. We apologize to all the researchers involved in the field who have not been cited in our manuscript for space limitation.

Author Contributions

Concept and design of the study: M.D. and S.H. Experimental procedures, data analysis, and writing: M.D., S.H., R.N., B.C., and Y.Y. The project was supervised by M.D.

Supporting Information Available

Supporting information is available as separate files (pdf and csv).

References

(1) Gilbert, W. Origin of life: The RNA world. *nature* **1986**, *319*, 618–618.

(2) Joyce, G. F. The antiquity of RNA-based evolution. *nature* **2002**, *418*, 214–221.

(3) Orgel, L. E. Evolution of the genetic apparatus. *Journal of molecular biology* **1968**, *38*, 381–393.

(4) Higgs, P. G.; N, L. The RNA World: molecular cooperation at the origins of life. *Nat Rev Genet* **2015**, *16*, 7–17.

(5) Lilley, D. M.; Huang, L. RNA catalysis moving towards metabolic reactions: progress with ribozyme catalyzed alkyl transfer. *Trends in Biochemical Sciences* **2025**,

(6) Seelig, B.; Chen, I. A. Intellectual frameworks to understand complex biochemical systems at the origin of life. *Nature Chemistry* **2025**, *17*, 11–19.

(7) Bernhardt, H. S. The RNA world hypothesis: the worst theory of the early evolution of life (except for all the others) a. *Biology direct* **2012**, *7*, 1–10.

(8) Robertson, M. P.; Joyce, G. F. The origins of the RNA world. *Cold Spring Harbor perspectives in biology* **2012**, *4*, a003608.

(9) Benner, S. A.; Kim, H.-J.; Yang, Z. Setting the stage: the history, chemistry, and geobiology behind RNA. *Cold Spring Harbor perspectives in biology* **2012**, *4*, a003541.

(10) Tekin, E.; Salditt, A.; Schwintek, P.; Wunnava, S.; Langlais, J.; Saenz, J.; Tang, D.; Schwille, P.; Mast, C.; Braun, D. Prebiotic foam environments to oligomerize and accumulate RNA. *ChemBioChem* **2022**, *23*, e202200423.

(11) Guseva, E.; Zuckermann, R. N.; Dill, K. A. Foldamer hypothesis for the growth and sequence differentiation of prebiotic polymers. *Proc Natl Acad Sci U S A* **2017**, *114*, E7460–E7468.

(12) Chatterjee, S.; Yadav, S. The origin of prebiotic information system in the peptide/RNA world: a simulation model of the evolution of translation and the genetic code. *Life* **2019**, *9*, 25.

(13) Guo, M.; Korenaga, J. Rapid rise of early ocean pH under elevated weathering rates. *Nature Geoscience* **2025**, *18*, 260–266.

(14) Li, M.; Huang, X.; Tang, T. D.; Mann, S. Synthetic cellularity based on non-lipid micro-compartments and protocell models. *Current opinion in chemical biology* **2014**, *22*, 1–11.

(15) Caschera, F.; Noireaux, V. Integration of biological parts toward the synthesis of a minimal cell. *Current opinion in chemical biology* **2014**, *22*, 85–91.

(16) Miller, D. M.; Gulbis, J. M. Engineering protocells: prospects for self-assembly and nanoscale production-lines. *Life* **2015**, *5*, 1019–1053.

(17) Szostak, J.; Bartel, D.; Luisi, P. Synthesizing life. *Nature* **2001**, *409*, 387–390.

(18) Cronin, L.; Walker, S. I. Beyond prebiotic chemistry. *Science* **2016**, *352*, 1174–1175.

(19) Martini, L.; Mansy, S. S. Cell-like systems with riboswitch controlled gene expression. *Chemical communications* **2011**, *47*, 10734–10736.

(20) Peters, R. J.; Louzao, I.; van Hest, J. C. From polymeric nanoreactors to artificial organelles. *Chemical Science* **2012**, *3*, 335–342.

(21) Dzieciol, A. J.; Mann, S. Designs for life: protocell models in the laboratory. *Chemical Society Reviews* **2012**, *41*, 79–85.

(22) Poudyal, R. R.; Pir Cakmak, F.; Keating, C. D.; Bevilacqua, P. C. Physical principles and extant biology reveal roles for RNA-containing membraneless compartments in origins of life chemistry. *Biochemistry* **2018**, *57*, 2509–2519.

(23) Hanczyc, M. M.; Fujikawa, S. M.; Szostak, J. W. Experimental models of primitive cellular compartments: encapsulation, growth, and division. *Science* **2003**, *302*, 618–622.

(24) Rahman, M. M.; Ueda, M.; Hirose, T.; Ito, Y. Spontaneous formation of gating lipid domain in uniform-size peptide vesicles for controlled release. *Journal of the American Chemical Society* **2018**, *140*, 17956–17961.

(25) Schreiber, A.; Huber, M. C.; Schiller, S. M. Prebiotic protocell model based on dynamic protein membranes accommodating anabolic reactions. *Langmuir* **2019**, *35*, 9593–9610.

(26) Litschel, T.; Ganzinger, K. A.; Movinkel, T.; Heymann, M.; Robinson, T.; Mutschler, H.; Schwille, P. Freeze-thaw cycles induce content exchange between cell-sized lipid vesicles. *New Journal of Physics* **2018**, *20*, 055008.

(27) Monnard, P.-A.; Deamer, D. W. Membrane self-assembly processes: Steps toward the first cellular life. *The Anatomical Record: An Official Publication of the American Association of Anatomists* **2002**, *268*, 196–207.

(28) Brangwynne, C. P.; Eckmann, C. R.; Courson, D. S.; Rybarska, A.; Hoege, C.; Gharakhani, J.; Jülicher, F.; Hyman, A. A. Germline P granules are liquid droplets that localize by controlled dissolution/condensation. *Science* **2009**, *324*, 1729–1732.

(29) Banani, S. F.; Lee, H. O.; Hyman, A. A.; Rosen, M. K. Biomolecular condensates: organizers of cellular biochemistry. *Nature reviews Molecular cell biology* **2017**, *18*, 285–298.

(30) Agrawal, A.; Radakovic, A.; Vonteddu, A.; Rizvi, S.; Huynh, V. N.; Douglas, J. F.; Tirrell, M. V.; Karim, A.; Szostak, J. W. Did the exposure of coacervate droplets to rain make them the first stable protocells? *Science Advances* **2024**, *10*, eadn9657.

(31) Abbas, M.; Lipiński, W. P.; Nakashima, K. K.; Huck, W. T.; Spruijt, E. A short peptide synthon for liquid–liquid phase separation. *Nature Chemistry* **2021**, *13*, 1046–1054.

(32) Matsuo, M.; Kurihara, K. Proliferating coacervate droplets as the missing link between chemistry and biology in the origins of life. *Nature Communications* **2021**, *12*.

(33) Donau, C.; Späth, F.; Sosson, M.; Kriebisch, B. A. K.; Schnitter, F.; Tena-Solsona, M.; Kang, H.-S.; Salibi, E.; Sattler, M.; Mutschler, H.; Boekhoven, J. Active coacervate droplets as a model for membraneless organelles and protocells. *Nature Communications* **2020**, *11*.

(34) Jiang, L.; Zeng, Y.; Li, H.; Lin, Z.; Liu, H.; Richardson, J. J.; Gao, Z.; Wu, D.; Liu, L.; Caruso, F.; Zhou, J. Peptide-Based Coacervate Protocells with Cytoprotective Metal–Phenolic Network Membranes. *Journal of the American Chemical Society* **2023**, *145*, 24108–24115, PMID: 37788442.

(35) Abbas, M.; Lipiński, W. P.; Wang, J.; Spruijt, E. Peptide-based coacervates as biomimetic protocells. *Chem. Soc. Rev.* **2021**, *50*, 3690–3705.

(36) Aumiller Jr, W. M.; Keating, C. D. Phosphorylation-mediated RNA/peptide complex coacervation as a model for intracellular liquid organelles. *Nature chemistry* **2016**, *8*, 129–137.

(37) Ianeselli, A.; Tetiker, D.; Stein, J.; Kühnlein, A.; Mast, C. B.; Braun, D.; Dora Tang, T.-Y. Non-equilibrium conditions inside rock pores drive fission, maintenance and selection of coacervate protocells. *Nature chemistry* **2022**, *14*, 32–39.

(38) Matsuo, M.; Kurihara, K. Proliferating coacervate droplets as the missing link between chemistry and biology in the origins of life. *Nature communications* **2021**, *12*, 5487.

(39) Dindo, M.; Bevilacqua, A.; Soligo, G.; Calabrese, V.; Monti, A.; Shen, A. Q.; Rosti, M. E.; Laurino, P. Chemotactic interactions drive migration of membraneless active droplets. *Journal of the American Chemical Society* **2024**, *146*, 15965–15976.

(40) Testa, A.; Dindo, M.; Rebane, A. A.; Nasouri, B.; Style, R. W.; Golestanian, R.; Dufresne, E. R.; Laurino, P. Sustained enzymatic activity and flow in crowded protein droplets. *Nature communications* **2021**, *12*, 6293.

(41) Dindo, M.; Metson, J.; Ren, W.; Chatzittofi, M.; Yagi, K.; Sugita, Y.; Golestanian, R.; Laurino, P. Enzymes can activate and mobilize the cytoplasmic environment across scales. *bioRxiv* **2025**, 2025.01.28.635259.

(42) Fine, J. L.; Moses, A. M. An RNA condensate model for the origin of life. *Journal of Molecular Biology* **2025**, 169124.

(43) Smith, A. E.; Bellware, F. T.; J, S. J. Formation of nucleic acid coacervates by dehydration and rehydration. *Nature* **1967**, *214*, 1038–1040.

(44) Ramachandran, V.; Potoyan, D. Molecular Drivers of RNA Phase Separation. *bioRxiv* **2025**, 2025.01.20.633842.

(45) Onuchic, P. L.; Milin, A. N.; Alshareedah, I.; Deniz, A. A.; Banerjee, P. R. Divalent cations can control a switch-like behavior in heterotypic and homotypic RNA coacervates. *Scientific reports* **2019**, *9*, 12161.

(46) Wang, W.-J.; Tan, C.-P.; Mao, Z.-W. Metals and inorganic molecules in regulating protein and nucleic acid phase separation. *Current Opinion in Chemical Biology* **2023**, *74*, 102308.

(47) Van Treeck, B.; Protter, D. S.; Matheny, T.; Khong, A.; Link, C. D.; Parker, R. RNA self-assembly contributes to stress granule formation and defining the stress granule transcriptome. *Proceedings of the National Academy of Sciences* **2018**, *115*, 2734–2739.

(48) Rissone, P.; Severino, A.; Pastor, I.; Ritort, F. Universal cold RNA phase transitions. *Proceedings of the National Academy of Sciences* **2024**, *121*, e2408313121.

(49) Lipfert, J.; Doniach, S.; Das, R.; Herschlag, D. Understanding Nucleic Acid–Ion Interactions. *Annual Review of Biochemistry* **2014**, *83*, 813–841.

(50) Wadsworth, G. M.; Zahurancik, W. J.; Zeng, X.; Pullara, P.; Lai, L. B.; Sidharthan, V.; Pappu, R. V.; Gopalan, V.; Banerjee, P. R. RNAs undergo phase transitions with lower critical solution temperatures. *Nature Chemistry* **2023**, *15*, 1693–1704.

(51) Valdes-Garcia, G.; Gamage, K.; Smith, C.; Martirosova, K.; Feig, M.; Lapidus, L. J. The effect of polymer length in liquid-liquid phase separation. *Cell Reports Physical Science* **2023**, *4*, 101415.

(52) Choi, J.-M.; Holehouse, A. S.; Pappu, R. V. Physical Principles Underlying the Complex Biology of Intracellular Phase Transitions. *Annual Review of Biophysics* **2020**, *49*, 107–133.

(53) Papastavrou, N.; Horning, D. P.; Joyce, G. F. RNA-catalyzed evolution of catalytic RNA. *Proceedings of the National Academy of Sciences* **2024**, *121*, e2321592121.

(54) Jia, T. Z.; Hentrich, C.; Szostak, J. W. Rapid RNA exchange in aqueous two-phase system and coacervate droplets. *Origins of Life and Evolution of Biospheres* **2014**, *44*, 1–12.

(55) Fares, H. M.; Marras, A. E.; Ting, J. M.; Tirrell, M. V.; Keating, C. D. Impact of wet-dry cycling on the phase behavior and compartmentalization properties of complex coacervates. *Nature communications* **2020**, *11*, 5423.

(56) Joyce, G. F.; Szostak, J. W. Protocells and RNA Self-Replication. *Cold Spring Harbor Perspectives in Biology* **2018**, *10*, a034801.

(57) Wolf, Y. I.; Koonin, E. V. On the origin of the translation system and the genetic code in the RNA world by means of natural selection, exaptation, and subfunctionalization. *Biology Direct* **2007**, *2*, 14.

(58) Korn, E. D.; Carlier, M.-F.; Pantaloni, D. Actin polymerization and ATP hydrolysis. *Science* **1987**, *238*, 638–644.

(59) Testa, B.; Mayer, J. M. *Hydrolysis in drug and prodrug metabolism*; John Wiley & Sons, 2003.

(60) Guo, X.; Farag, M.; Qian, N.; Yu, X.; Ni, A.; Ma, Y.; Yu, W.; King, M. R.; Liu, V.; Lee, J.; others Biomolecular condensates can function as inherent catalysts. *bioRxiv* **2024**, 2024.07.06.602359.

(61) Rai, S.; Pramanik, S.; Mukherjee, S. Deciphering the liquid–liquid phase separation induced modulation in the structure, dynamics, and enzymatic activity of an ordered protein β-lactoglobulin. *Chemical Science* **2024**, *15*, 3936–3948.

(62) Springsteen, G.; Yerabolu, J. R.; Nelson, J.; Rhea, C. J.; Krishnamurthy, R. Linked cycles of oxidative decarboxylation of glyoxylate as protometabolic analogs of the citric acid cycle. *Nature communications* **2018**, *9*, 91.

(63) Eckhardt, A. K.; Bergantini, A.; Singh, S. K.; Schreiner, P. R.; Kaiser, R. I. Formation of Glyoxylic Acid in Interstellar Ices: A Key Entry Point for Prebiotic Chemistry. *Angewandte Chemie International Edition* **2019**, *58*, 5663–5667.

(64) Eschenmoser, A. On a Hypothetical Generational Relationship between HCN and Constituents of the Reductive Citric Acid Cycle. *Chemistry & Biodiversity* **2007**, *4*, 554–573.

(65) Chimiak, L.; Hara, E.; Sessions, A.; Templeton, A. Glycine synthesis from nitrate and glyoxylate mediated by ferroan brucite: An integrated pathway for prebiotic amine synthesis. *Proceedings of the National Academy of Sciences* **2024**, *121*.

(66) Baruch Leshem, A.; Sloan-Dennison, S.; Massarano, T.; Ben-David, S.; Graham, D.; Faulds, K.; Gottlieb, H. E.; Chill, J. H.; Lampel, A. Biomolecular condensates formed by designer minimalistic peptides. *Nature Communications* **2023**, *14*, 421.

(67) Paige, J. S.; Wu, K. Y.; Jaffrey, S. R. RNA Mimics of Green Fluorescent Protein. *Science* **2011**, *333*, 642–646.

(68) Chen, X. et al. Visualizing RNA dynamics in live cells with bright and stable fluorescent RNAs. *Nature Biotechnology* **2019**, *37*, 1287–1293.

(69) Ganim, Z.; Rief, M. Mechanically switching single-molecule fluorescence of GFP by unfolding and refolding. *Proceedings of the National Academy of Sciences* **2017**, *114*, 11052–11056.

(70) Conter, C.; Oppici, E.; Dindo, M.; Rossi, L.; Magnani, M.; Cellini, B. Biochemical properties and oxalate-degrading activity of oxalate decarboxylase from bacillus subtilis at neutral pH. *IUBMB life* **2019**, *71*, 917–927.

(71) Dindo, M.; Conter, C.; Uechi, G.-I.; Pampalone, G.; Ruta, L.; Pey, A. L.; Rossi, L.; Laurino, P.; Magnani, M.; Cellini, B. Engineered Oxalate Decarboxylase Boosts Activity and Stability for Biological Applications. *ACS Omega* **2025**, *10*, 12375–12384.

(72) Poudyal, R. R.; Guth-Metzler, R. M.; Veenis, A. J.; Frankel, E. A.; Keating, C. D.; Bevilacqua, P. C. Template-directed RNA polymerization and enhanced ribozyme catalysis inside membraneless compartments formed by coacervates. *Nature Communications* **2019**, *10*, 490.

(73) Bernhardt, H. S.; Tate, W. P. Primordial soup or vinaigrette: did the RNA world evolve at acidic pH? *Biology Direct* **2012**, *7*, 4.

(74) Mariani, A.; Bonfio, C.; Johnson, C. M.; Sutherland, J. D. pH-Driven RNA Strand Separation under Prebiotically Plausible Conditions. *Biochemistry* **2018**, *57*, 6382–6386.

(75) Cottrell, J. W.; Scott, L. G.; Fedor, M. J. The pH Dependence of Hairpin Ribozyme Catalysis Reflects Ionization of an Active Site Adenine. *Journal of Biological Chemistry* **2011**, *286*, 17658–17664.

(76) Deshpande, K.; Kulshreshtha, N. N.; Mulewar, S. S.; Rajamani, S. Nucleotide-Protocell Interactions: A Reciprocal Relationship in Prebiotically Pertinent Environments. *ChemSystemsChem* **2024**, *6*.

(77) Krupka, H. I.; Huber, R.; Holt, S. C.; Clausen, T. Crystal structure of cystalysin from Treponema denticola: a pyridoxal 5'-phosphate-dependent protein acting as a haemolytic enzyme. *The EMBO journal* **2000**,

(78) Bertoldi, M.; Cellini, B.; Clausen, T.; Voltattorni, C. B. Spectroscopic and kinetic analyses reveal the pyridoxal 5 '-phosphate binding mode and the catalytic features of Treponema denticola cystalysin. *Biochemistry* **2002**, *41*, 9153–9164.